

CO₂ Treatment Enables Non-Hazardous, Reliable, and Efficacious Recovery of Spent Li(Ni_{0.5}Co_{0.2}Mn_{0.3})O₂ Cathodes

Longping Deng^{1, 2}, Zhuijun Xu², Mengmeng Wang², Huajian Shentu², Xiang Liu², Jianwei Xiong², Ya-Jun Cheng², Chao Wang³, Mingjiong Zhou¹, Jie Gao^{2*}, Yonggao Xia^{2, 4*}

1. The school of Materials Science and Chemical Engineering, Ningbo University, Ningbo 315211, P. R. China

2. Ningbo Institute of Materials Technology & Engineering, Chinese Academy of Sciences, 1219 Zhongguan West Rd, Ningbo, 315201, Zhejiang Province, P. R. China

3. School of Materials Science and Engineering, Tongji University, Shanghai 201804, China

4. Center of Materials Science and Optoelectronics Engineering, University of Chinese Academy of Sciences, 19A Yuquan Rd, Shijingshan District, Beijing 100049, P. R. China

E-mail: gaojie@nimte.ac.cn, xiayg@nimte.ac.cn

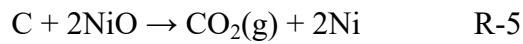
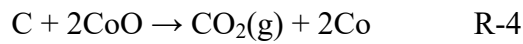
Reaction equilibrium analysis for carbothermal reaction in CO₂ atmosphere

The gas-phase equilibrium equation for the carbothermal reaction of pyrolysis products (NiO, and CoO) is calculated as follows.

Here, the isothermal equation for the chemical reaction is shown as follow:

$$\Delta_r G_m = \Delta_r G_m^\theta(T) + RT \ln Q = -RT \ln K_T^\theta + RT \ln Q \quad (1)$$

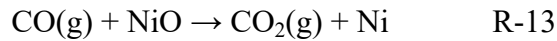
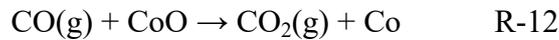
Direct reduction of MnO₂ by C:



The reaction quotient “Q_A” is calculated as follows:

$$Q_A = \frac{P(CO_2)}{P\theta}$$

Indirect reduction of MnO₂ by CO:



The reaction quotient “Q_A” is calculated as follows:

$$Q_A = \frac{\frac{P(CO_2)}{P\theta}}{\frac{P(CO)}{P\theta}}$$

Therefore, when the reaction reaches the equilibrium ($\Delta_r G_m = 0$), we can get the reaction quotient “Q_I” based on equation (1):

$$Q_I = K_T^\theta = \exp(-\Delta_r G_m^\theta(T) / (RT)) \quad (2)$$

If $Q_A < Q_I$, then $\Delta_r G_m < 0$, the reaction proceeds to the products side;

If $Q_A > Q_I$, then $\Delta_r G_m > 0$, the reaction shifts left toward the reactants;

If $Q_A = Q_I$, then $\Delta_r G_m = 0$, the reaction reaches dynamic equilibrium.

The greater the difference between the values of Q_A and Q_I, the greater the tendency for the reaction to proceed toward the products (or reactants).

Table S1 The standard Gibbs free energy ($\Delta_r G_m^\theta$) of direct (or indirect) carbothermal reaction of pyrolysis products (NiO, and CoO) in CO₂ temperatures

Temperature (°C)	Standard Gibbs Free Energy ($\Delta_r G_m^\theta$, kJ/mol)*			
	R-4	R-5	R-12	R-13
0	38.120	33.593	-43.133	-45.396
40	31.611	25.936	-42.876	-45.713
80	25.253	18.295	-42.514	-45.993
120	19.017	10.694	-42.072	-46.234
160	12.883	3.152	-41.567	-46.433
200	6.834	-4.315	-41.013	-46.587
240	0.860	-11.692	-40.418	-46.694
280	-5.049	-18.973	-39.791	-46.753
320	-10.901	-26.209	-39.138	-46.792
360	-16.703	-33.427	-38.464	-46.826
400	-22.461	-40.646	-37.773	-46.866
440	-28.201	-47.849	-37.080	-46.904
480	-33.935	-55.023	-36.390	-46.934
520	-39.639	-62.168	-35.692	-46.957
560	-45.317	-69.287	-34.989	-46.974
600	-50.973	-76.379	-34.282	-46.985
640	-56.610	-83.447	-33.573	-46.992
680	-62.231	-90.493	-32.864	-46.995
720	-67.839	-97.516	-32.157	-46.996
760	-73.438	-104.520	-31.452	-46.993
800	-79.031	-111.504	-30.752	-46.989
840	-84.620	-118.470	-30.058	-46.983
880	-90.209	-125.419	-29.371	-46.976
920	-95.800	-132.352	-28.693	-46.968
960	-101.398	-139.269	-28.025	-46.960
1000	-107.007	-146.171	-27.369	-46.951

* The value of the standard Gibbs free energy ($\Delta_r G_m^\theta$) is calculated by HSC-Chemistry

6.0.

Table S2 The reaction quotient “ Q_i ” of direct (or indirect) carbothermal reaction of pyrolysis products (NiO, and CoO) in CO₂ temperatures

Temperature (°C)	The reaction quotient “ Q_i ” *			
	R-4	R-5	R-12	R-13
0	5.13E-08	0.00	1.77E+08	4.80E+08
40	5.33E-06	0.00	1.42E+07	4.22E+07
80	1.84E-04	0.00	1.94E+06	6.36E+06
120	2.97E-03	0.04	3.89E+05	1.39E+06
160	0.03	0.42	1.03E+05	3.98E+05
200	0.18	3.00	33717.30	1.39E+05
240	0.82	15.49	13012.86	56657.16
280	3.00	61.91	5723.27	26009.27
320	9.12	203.31	2797.25	13207.23
360	23.88	572.57	1490.62	7299.13
400	55.33	1425.97	853.46	4332.81
440	116.33	3197.56	520.00	2726.27
480	225.76	6550.18	334.12	1799.70
520	407.96	12427.53	224.22	1237.52
560	693.86	22085.43	156.21	881.32
600	1120.64	37103.00	112.44	647.00
640	1731.15	59372.41	83.28	487.73
680	2573.32	91068.63	63.26	376.31
720	3699.36	1.35E+05	49.13	296.36
760	5165.03	1.93E+05	38.93	237.68
800	7029.05	2.68E+05	31.40	193.74
840	9352.78	3.63E+05	25.73	160.24
880	12200.10	4.80E+05	21.40	134.27
920	15637.80	6.23E+05	18.04	113.84
960	19736.21	7.93E+05	15.39	97.55
1000	24570.65	9.94E+05	13.27	84.41

* The value of the reaction quotient “ Q_i ” is calculated according to Equation (2).

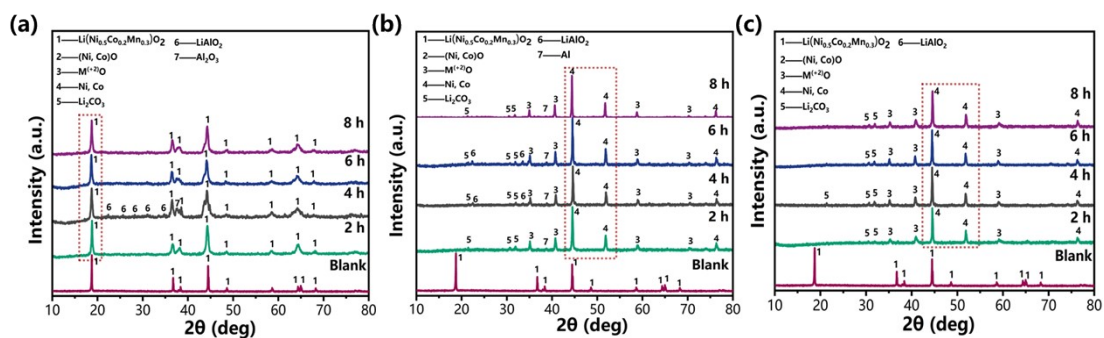


Figure S1. XRD patterns of the cathode materials after thermal reduction at 600 °C for different heating times in (a) air, (b) Ar, and (c) H₂/Ar atmosphere.

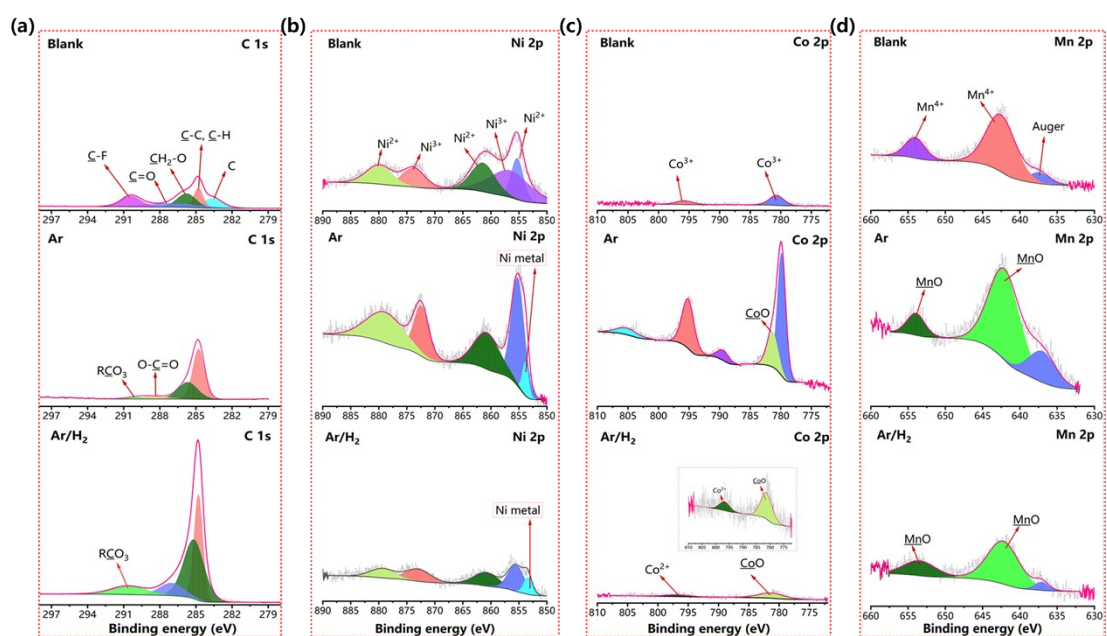


Figure S2. XPS spectra of (a) C 2s, (b) Ni 2p, (c) Co 2p, and (d) Mn 2p for the pristine (blank) and the cathode thermally treated in Ar, and H₂/Ar atmospheres (thermal-treat temperature: 600 °C, and heating time: 4h).

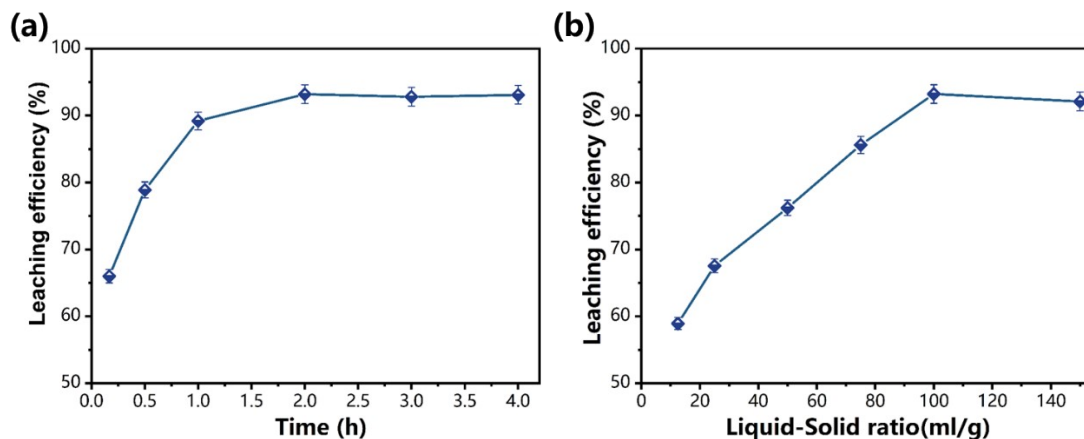


Figure S3. Effects of (a) leaching time, (b) liquid-solid ratio on the efficiency of water leaching of lithium.

The effect of time on the water leaching of lithium components is shown in **Figure S3a**. The leaching efficiency of lithium is only 65.99 % when the leaching time is 10 minutes. When the leaching time increases, the lithium leaching efficiency increases significantly. When the leaching time is increased to 2 h, the leaching efficiency of lithium reaches 93.22 %. With a further increase of leaching time, the improvement of the leaching efficiency is almost negligible. Considering the leaching efficiency of lithium and energy consumption, the best leaching time is determined as 2 h.

The solubility of Li_2CO_3 is only 13.3 g/L at 20 °C, which limits the efficiency of selective extraction of the lithium fraction from the heat-treated cathode scrap.¹ Therefore, the influence of different liquid-solid ratios on water-leaching lithium components is explored (**Figure S3b**). At a liquid-solid ratio of 12.5 ml/g, the lithium leaching efficiency was only 58.93 %. The leaching efficiency of lithium gradually increases with the increase of the liquid-solid ratio and reaches 93.22 % with the liquid-solid ratio of 100 ml/g. With further increasing liquid-solid ratio, the leaching efficiency

does not change significantly. Considering the leaching efficiency of lithium and the lithium concentration of the leaching solution, the optimal liquid-solid ratio is determined to be 100 ml/g.

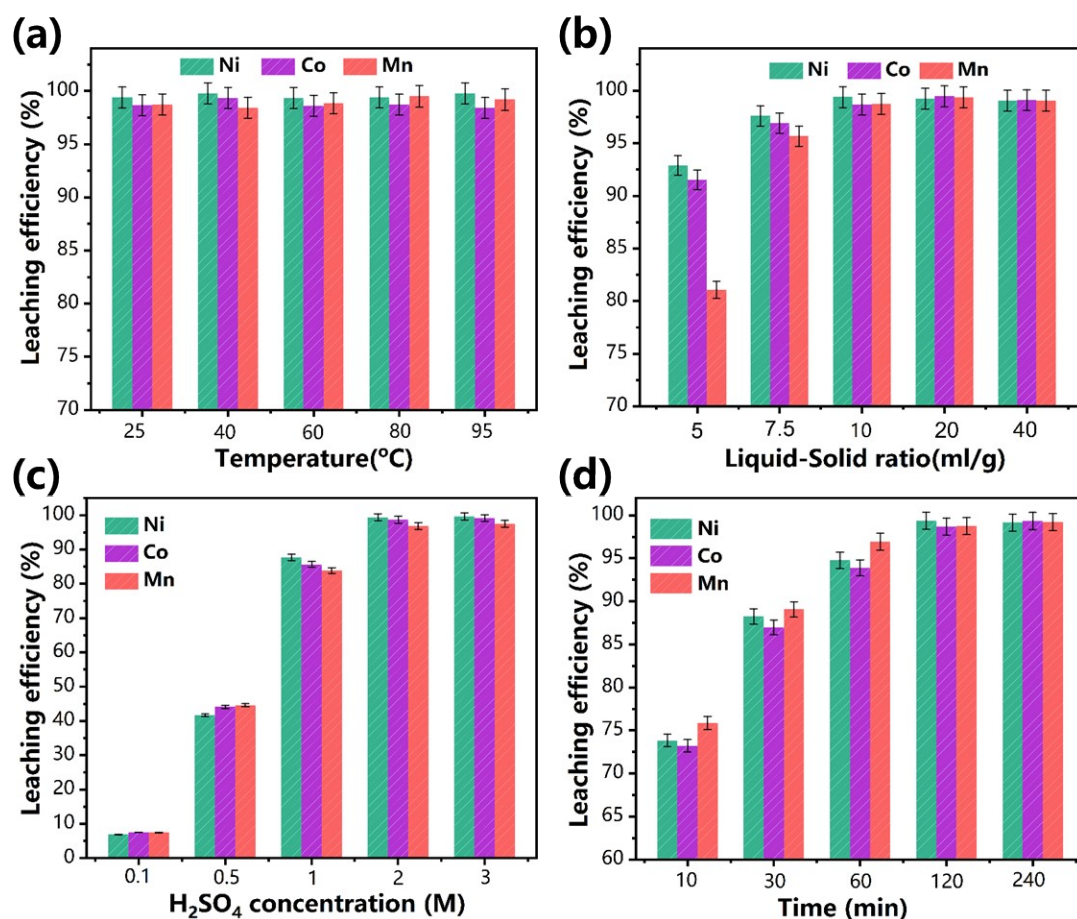


Figure S4. Effects of (a) H₂SO₄ concentration, (b) liquid-solid ratio, (c) leaching temperature, and (d) leaching time on the leaching efficiency.

The valuable Ni, Co and Mn components are retained in the residue after the water leaching. Here, the Ni, Co and Mn components are further extracted by sulfuric acid leaching. A series of experiments are performed to obtain the best leaching conditions as shown in **Figure S4**.

Figure S4a shows the effect of sulfuric acid concentration on the leaching

efficiency of Ni, Co, and Mn under the following conditions: leaching time of 2 h, the liquid-solid ratio of 10 ml/g, and reaction temperature of 25 °C. The leaching efficiencies of Ni, Co and Mn are 6.90 %, 7.52 % and 7.48 % for the sulfuric acid concentration of 0.1 M, while the leaching efficiencies of Ni, Co and Mn are increased with increasing sulfuric acid concentration. This may be attributed to the fact that the increase in acid concentration improves the collision frequency between the reactants, thus speeding up the reaction.² The leaching efficiency reaches its maximum when the sulfuric acid concentration reaches 2 M, and the leaching efficiencies of Ni, Co and Mn all increase to 99.39 %, 98.69 % and 98.75 %. With a further increase in sulfuric acid concentration to 3 M, the leaching efficiency is hardly changed. Therefore, 2 M is determined as the optimum concentration of sulfuric acid.

By fixing the sulfuric acid concentration at 2 M, the leaching time of 2 h and the reaction temperature at 25 °C, the effect of liquid-solid ratio on the leaching efficiency of Ni, Co and Mn is studied. In **Figure S4b**, the leaching efficiency of Ni, Co and Mn is 92.90 %, 91.53 % and 81.09 % for a liquid-solid ratio of 5 ml/g, and the leaching efficiency of Ni, Co and Mn increases with increasing liquid-solid ratio. This may be related to the increase in the liquid-solid ratio, which decreases the available surface area per unit volume of solution.³ When the liquid-solid ratio reaches 10 ml/g, the leaching efficiency of Ni, Co and manganese are all increased to 99.39 %, 98.69 % and 98.75 %. However, within the range of 10-40 ml/g, the leaching efficiencies of Ni, Co and Mn are almost constant. Therefore, 10 ml/g is determined as the optimized liquid-solid ratio.

By fixing the sulfuric acid concentration at 2 M, the liquid-solid ratio at 10 ml/g and the leaching time at 2 h, the effect of reaction temperature on the leaching efficiency of Ni, Co and Mn is studied. When the reaction temperature is 25 °C, the leaching efficiencies of Ni, Co and Mn are 99.39 %, 98.69 %, and 98.75 % (**Figure S4c**). But there is almost no change in the leaching efficiency during the increase of the reaction temperature to 95 °C. This may be due to the fact that the low-valent oxides (Ni, Co, and Mn) react easily with sulfuric acids. While the exothermic reaction allows the leaching reaction of metal ions to proceed thoroughly at room temperature (25 °C). Therefore, 25 °C is defined as the optimal reaction temperature.

By fixing the sulfuric acid concentration at 2 M, the liquid-solid ratio at 10 ml/g and the reaction temperature at 25 °C, the effect of leaching time on the leaching efficiency of Ni, Co, and Mn is studied. In **Figure S4d**, the leaching efficiencies of Ni, Co, and Mn are 73.83 %, 73.21 %, and 75.88 % at a leaching time of 10 minutes, and a significant increase in the leaching efficiency of metal ions occurs with the leaching time increased to 2 h. Ultimately, the leaching efficiency of Co and Mn reaches 99.39 %, 98.69 % and 98.75 %. And the increase in leaching time does not have a significant impact on the leaching efficiency. To obtain high leaching efficiency in a short time, 2 h is determined as the best leaching time.

Table S3. Summary of operating conditions for leaching of valuable metals from spent lithium-ion batteries.

sample	Condition	Method	Recovery rate (%)	Ref.
In this study				
NCM	CO ₂ , 600 °C, 4h	Li: water leaching; Ni, Co and Mn: Acid leaching (25 °C)	92.84% Li, 99.39% Ni, 98.69% Co, 98.75% Mn	-
NCM	air, 600 °C, 4h		27.32% Li, 26.16% Ni, 21.75% Co, 27.53% Mn	-
NCM	Ar, 600 °C, 4h		91.23% Li, 85.80% Ni, 84.78% Co, 98.66% Mn	-
NCM	H ₂ /Ar, 600 °C, 4h		86.98% Li, 85.48% Ni, 85.11% Co, 98.98% Mn	-
Priority extraction of Li components				
NCM	Ar, 600 °C, 4h, 19.9% Lignite	Water leaching	84.7% Li	4
LMO	Vacuum, 800 °C, 45min, Graphite	Water leaching	91.30% Li	5
LCO	Ar, 600 °C, 1h, Al collector	NaOH solution leaching	93.67% Li	6
NCM	Ar, 650 °C, 3h, 20% Carbon	Water leaching (CO ₂)	80% Li	7
NCM	Na ₂ S 9H ₂ O	Ball milling; water leaching	95.10% Li	8
Extraction of Ni, Co, and Mn components				
NCM	2 M H ₂ SO ₄ , 3 vol% H ₂ O ₂	Acid leaching (60 °C)	99% Ni, 99% Co, 99% Mn	9
NCM	3.5 M H ₂ SO ₄	Acid leaching (85 °C)	99.9% Ni, 99.4% Co, 99.7% Mn	4
NCM	0.5 M H ₂ SO ₄ , 0.1 M Na ₂ SO ₃	Hydrothermal (120 °C)	93.11% Ni, 92.84% Co, 90.18% Mn	10
NCM	2M L-tartaric acid, 4 vol% H ₂ O ₂	Acid leaching (70 °C)	99.31% Ni, 92.84% Co, 99.31% Mn	2
NCM	2 M H ₃ PO ₄ , 4 vol% H ₂ O ₂	Acid leaching (60 °C)	99.5% Ni, 96.3% Co, 98.8% Mn	11

LCO: LiCoO₂; NCM: LiNi_xCo_yMn_zO₂; LMO: LiMnO₂

Comparison of leaching efficiency with different conditions was provided in Table S3, CO₂ treatment with high leaching efficiency of Li, Ni, Co and Mn in preferential Li extraction and transition metals (Ni, Co and Mn) extraction was achieved at 25 °C.

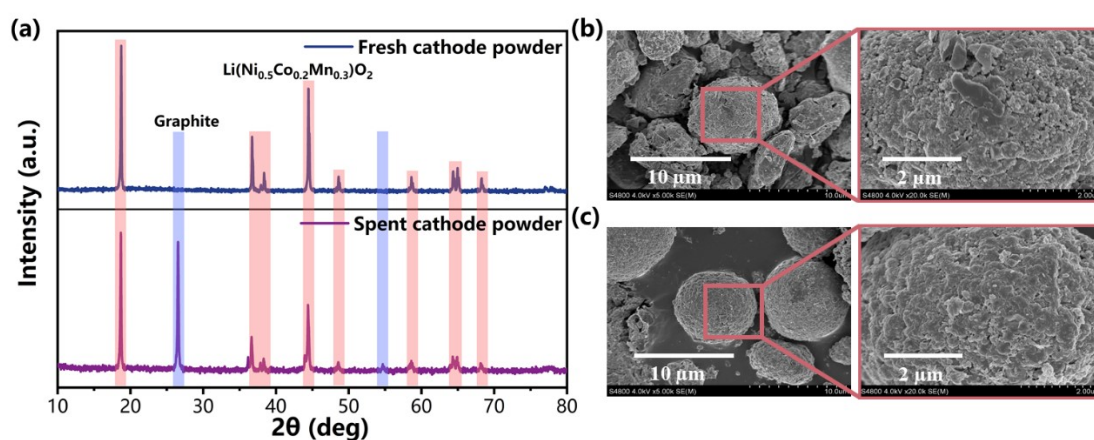


Figure S5. (a) XRD patterns of the home-made and spent cathode powder. SEM images

of (b) spent and (c) home-made cathode powder.

XRD diffraction was used to explore the structural differences between spent and home-made cathode powders. As shown by **Figure S5a**, the diffraction peaks representing lithium cobaltate appear in both spent and home-made cathode powders. It indicates that the major phase is retained in the spent cathode. However, peaks from graphite impurity are observed in the spent cathode powder, which is related to the commingling of the cathode and anode powders in the pre-treatment process. Spherical secondary particles with porous and loose surfaces together with broken irregular particles are observed by SEM (**Figure S5(b)** and **(c)**), which resemble their shape in the home-made cathode powder. It suggests that the recycling method developed in this work on the home-made cathode powder is potentially applicable to the spent cathode powder, even though the exact optimized condition may be modified.

References

1. P. Liu, L. Xiao, Y. Chen, Y. Tang, J. Wu and H. Chen, *J Alloy Compd*, 2019, **783**, 743-752.
2. L.-P. He, S.-Y. Sun, Y.-Y. Mu, X.-F. Song and J.-G. Yu, *ACS Sustain Chem Eng*, 2016, **5**, 714-721.
3. M. K. Jha, A. Kumari, A. K. Jha, V. Kumar, J. Hait and B. D. Pandey, *Waste Manage*, 2013, **33**, 1890-1897.
4. J. Hu, J. Zhang, H. Li, Y. Chen and C. Wang, *J Power Sources*, 2017, **351**, 192-199.
5. J. Xiao, J. Li and Z. Xu, *J Hazard Mater*, 2017, **338**, 124-131.
6. W. Wang, Y. Zhang, X. Liu and S. Xu, *ACS Sustain Chem Eng*, 2019, **7**, 12222-12230.
7. J. Zhang, J. Hu, W. Zhang, Y. Chen and C. Wang, *J Clean Prod*, 2018, **204**, 437-446.
8. Y. Yang, H. Yang, H. Cao, Z. Wang, C. Liu, Y. Sun, H. Zhao, Y. Zhang and Z. Sun, *J Clean Prod*, 2019, **236**.
9. T. Liu, J. Chen, H. Li and K. Li, *Sep Purif Technol*, 2020, **245**.
10. X. Tang, W. Tang, J. Duan, W. Yang, R. Wang, M. Tang and J. Li, *J Alloy Compd*, 2021, **874**.
11. X. Chen, J. Li, D. Kang, T. Zhou and H. Ma, *Green Chemistry*, 2019, **21**, 6342-6352.